Perpendicular and in-plane magnetic anisotropy in epitaxial Cu/Ni/Cu/Si(111) ultrathin films

G. Gubbiotti, G. Carlotti, and G. Socino
Dipartimento di Fisica dell'Università, Istituto Nazionale per la Fisica della Materia, Via Pascoli, I-06100 Perugia, Italy

F. D'Orazio and F. Lucari
Dipartimento di Fisica dell'Università, Istituto Nazionale per la Fisica della Materia, Via Vetoio, I-67010 Coppito (L'Aquila), Italy

R. Bernardini and M. De Crescenzi
Dipartimento di Matematica e Fisica dell'Università, Istituto Nazionale per la Fisica della Materia, Via Madonna delle Carceri, I-62032 Camerino, Italy

(Received 17 April 1997)

Epitaxial ultrathin Cu/Ni/Cu films with Ni thickness in the range 1.5–6 nm have been grown by UHV evaporation on the Si(111)-7×7 surface. *In situ* characterization made by low-energy electron diffraction and Kikuchi electron diffraction revealed that both Ni and Cu films grow epitaxially on Si, with a (111) orientation and with their (110) axis parallel to the (121) axis of the Si substrate. Magneto-optical Kerr effect measurements performed at room temperature have shown that the preferential direction of magnetization lies in the film plane for Ni thickness above 3 nm, while it is perpendicular to the film plane for lower thickness. Brillouin light scattering was then exploited to study the spin-wave dispersion as a function of both the applied magnetic field and the wave vector direction on the surface plane. In order to interpret the Brillouin data, we have used a macroscopic model which takes into account both dipolar and exchange interactions, as well as bulk and interface anisotropy for the (111) plane of a cubic crystal. This enabled us to determine, in addition to the other magnetic parameters, both the in-plane and the out-of-plane anisotropy constants. The observed dependence of these constants on the film thickness indicates that the magnetic anisotropy is mainly of magnetoelastic origin. [S0163-1829(97)07838-7]

I. INTRODUCTION

In recent years a great effort has been devoted to the study of magnetic films and multilayers in which there is a change of the preferential orientation of the magnetization from the commonly observed in-plane direction to that perpendicular to the film plane. This phenomenon, usually referred to as perpendicular magnetic anisotropy (PMA), originates from the competition between the magnetostatic energy and the out-of-plane anisotropy energy. Using this effect, it is possible to tailor and synthesize structures in which the magnetization can be normal or parallel to the film, by varying the thickness of the magnetic film and choosing an appropriate combination of materials. This is very important for technological applications such us solid-state electronic devices and magnetic recording media. As a consequence, several experimental techniques capable of investigating the magnetic properties of ultrathin films have been developed. Among these, the Brillouin-light-scattering (BLS) technique, based on the inelastic scattering of photons by thermally excited spin waves (thermal magnons), has proved to be the most powerful technique for studying spin waves in two-dimensional systems, with a sensitivity down to the monolayer scale.[1] It has been shown that BLS measurements give access to the determination of magnetic parameters and magnetic anisotropy constants and allow one to obtain information on the magnetization orientation with respect to the film plane.[1] All the previous BLS investigations of ultrathin magnetic structures were mainly concerned with Fe (Refs. 2 and 3) and Co,[3,4] while no BLS investigation of magnetic anisotropy in Ni ultrathin films has been reported to date in the literature.[3] This lack of Brillouin data on Ni is probably motivated also by the relatively small Brillouin cross section with respect to other ferromagnetic materials.[5] In spite of this, Ni films are very appealing in the study of magnetic anisotropy, because Ni has a relatively small magnetostatic energy density (the magnetostatic energy constant is an order of magnitude lower than that of Fe) which constitutes the main resistance to perpendicular magnetization.

In this paper we present the results of a BLS analysis of magnetic anisotropy of epitaxial Cu/Ni/Cu heterostructures, for different thicknesses of the Ni layer, deposited by UHV evaporation on a Si(111) substrate. We have chosen to deposit the Ni magnetic ultrathin films on Si(111) because of the large literature existing on Cu and Ni metallic depositions on such a surface at room temperature which ensures about the quasiperfect pseudomorphic growth along the (111) direction.[6] On the other hand, Tonner *et al.*[7] concluded, through x-ray photoelectron diffraction (XPD) measurements, that Cu epitaxy does not occur on Si(100) even at the early stage of the interface formation, in strong contrast with the results previously reported by Chang.[8] In addition, to best of our knowledge no previous BLS investigations of magnetic anisotropies in ultrathin ferromagnetic films with (111) orientation have been reported in the literature except for the work made by Hillebrands *et al.* on Co(111) ultrathin films where no in-plane anisotropy could be observed.[9] The structural and magnetic characterization of our films has been performed by *in situ* electron spectroscopy techniques and by the *ex situ* magneto-optical Kerr effect (MOKE), re-

spectively. With this information in hand, the dispersion of the spin-wave frequency with both the strength of the applied magnetic field and the wave vector direction on the surface plane has been studied by BLS. In order to interpret the BLS data, the approaches previously proposed by Stamps and Hillebrands[10–12] for the calculation of the spin-wave frequency in magnetic ultrathin films have been extended to the case of a cubic film with (111) surface orientation. This enabled us to analyze the magnetization orientation and to determine the magnetic parameters of the film, including the in-plane and the out-of-plane magnetic anisotropy constants.

The plan of the paper is as follows. Section II is devoted to the description of the specimen preparation and the *in situ* structural characterization. In Sec. III, we present the MOKE and BLS techniques which provide information about both the static and the dynamic properties of the magnetization. The theoretical models we use for the calculation of the spin-wave frequency measured in BLS spectra as a function of the applied magnetic field and of the wave vector direction on the surface plane are described in Sec. IV. In Sec. V the experimental results are presented and discussed, while conclusions are outlined in the last Sec. VI.

II. SAMPLE PREPARATION AND STRUCTURAL CHARACTERIZATION

A. Sample growth conditions

The Ni ultrathin films used in the present experiment were grown in a UHV chamber operating at Camerino University. The pressure during Ni depositions rose from a base value of 2×10^{-10} Torr to a few 10^{-9} Torr. The substrate was an optically polished Si(111) crystal (p type, 0.1 Ω cm) clamped on two rods for direct Joule heating. The atomic cleaning was obtained by a series of successive flashes at 1200 °C to get an *in situ* desorption of the native oxide. To reach such a temperature a current of 8 A flowing through the sample was required. The nominal thickness of each deposited layer was monitored *in situ* by means of an INFICON quartz microbalance. To obtain the best conditions of epitaxial growth, a Cu buffer layer 3.5 nm thick was deposited at room temperature on the clean Si substrate before every Ni evaporation. This procedure was aimed to relax the in-plane strain which arises from the huge lattice mismatch at the interface with the Si substrate and to avoid the formation of Ni silicides and/or metallic islands. Successive Ni layers were evaporated onto the substrate, kept at room temperature, by flowing a current of 13 A in a Ni filament (purity 99.999%) of 1 mm diameter. Various Ni films of different thickness were grown in these conditions and the samples studied in this work are listed in Table I. In order to prevent Ni layers from oxygen contamination during *ex situ* measurements, a Cu protective capping layer, 3.5 nm thick, was deposited on top of the Ni film. The growth rate, for both Cu and Ni, was about 0.1 nm/s. The coating of Ni films with Cu as well as the cleanliness of the Si substrate was controlled by Auger spectroscopy, low-energy electron diffraction (LEED), and Kikuchi electron diffraction (KED), as discussed below. Further details of the experimental UHV apparatus have been reported elsewhere.[13]

TABLE I. Magnetic parameters of the Cu/Ni/Cu/Si(111) heterostructures deduced by BLS.

Sample No.	d (nm)	M_s (Oe)	K_s (erg/cm^2)	K_p (erg/cm^2)
1	1.5	483 ± 8	0.116 ± 0.002	
2	2.0	480 ± 6	0.174 ± 0.002	
3	2.5	480 ± 8	0.190 ± 0.002	0.060 ± 0.008
4	3.0	470 ± 6	0.210 ± 0.002	0.070 ± 0.008
5	6.0	478 ± 7	0.380 ± 0.002	0.150 ± 0.008

B. Atomic and structural surface characterization

Figure 1(a) shows the Auger spectrum taken after the cleaning procedure of the Si substrate with an $L_{2,3}VV$ (92 eV) Auger transition. Neither carbon nor oxygen or any other contaminants were detected within the Auger atomic sensitivity. In this way the degree of cleaning is estimated to be better than 0.5%. Figures 1(b), 1(c), and 1(d) show the typical Auger spectra taken at the different stages of Cu, Ni, and final Cu deposition. Sizable interdiffusion between metals and silicon or formation of metallic islands can be excluded because only the characteristic Auger features of the deposited materials have been observed.

The structural surface characterization made by LEED and KED has revealed that both Cu and Ni films grow epitaxially on Si with (111) orientation, but their (110) axis is parallel to the (121) axis of the Si substrate. This 30° rotation reduces the huge lattice mismatch (33%) between Cu and Si to approximately 16%. In Fig. 2(a) a LEED image of the Si(111) substrate, showing the characteristic 7×7 recon-

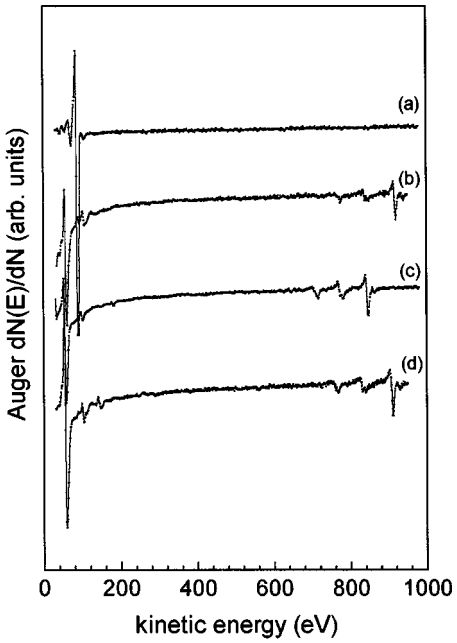

FIG. 1. Auger spectra for sample No. 2: (a) Auger signal of the Si(111)7×7 surface after cleaning procedure described in the text, (b) Auger signal of the 3.5-nm-thick Cu buffer layer deposited onto the Si substrate, (c) Auger signal after the deposition of 2.0 nm of Ni onto the Cu buffer layer (note the absence of features characteristic of Cu atoms and of alloy formation at the interface), and (d) after the deposition of the 3.5-nm-thick Cu overlayer.

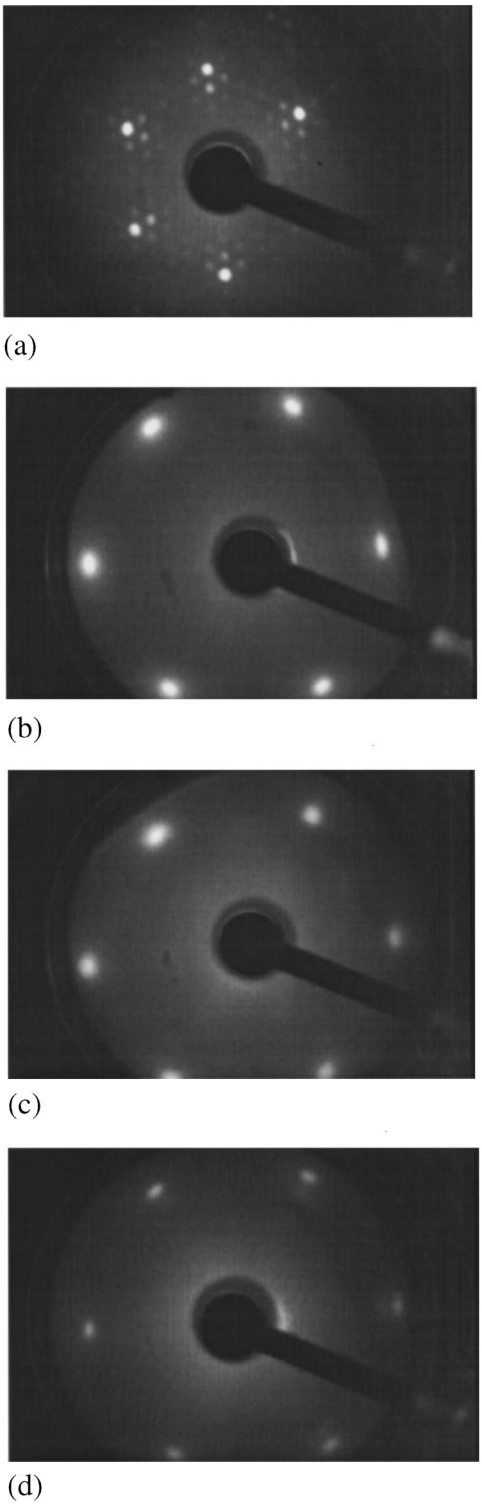

FIG. 2. LEED patterns of each layer of the Cu/Ni/Cu/Si(111) heterostructure with Ni thickness of 2.0 nm (sample No. 2) taken at the same energy of the primary electron beam of 56 eV. (a) LEED image of the Si(111)-7×7 reconstructed surface, (b) of the Cu buffer layer, (c) of the Ni layer, and (d) of the Cu overlayer. The 30° rotation between the Si substrate and the Cu buffer layer can be easily recognized by a comparison of patterns (a) and (b).

structed pattern, is reported. Figure 2(b) shows the LEED pattern of the Cu buffer layer 3.5 nm thick grown on the Si substrate. The comparison between Figs. 2(a) and 2(b) clearly reveals the 30° rotation between the Cu layer and the Si substrate and loss of surface reconstruction. All the LEED patterns shown in Fig. 2 were taken at the same energy of the primary beam of 56 eV. From LEED images, the typical sixfold symmetry of the (111) plane for both Cu and Ni layers can be easily recognized. This means that the Cu/Si(111) interface formation, in which the Cu atoms reside in every hollow site of the 1×1 unreconstructed Si substrate,[14] dictates the epitaxial growth of all the successive metallic layers. However, a semiquantitative estimation of the LEED spots position reveals that the 3.5-nm-thick Cu buffer has relaxed about 85–90 % of the nominal strain (16%) which would result from pseudomorphic growth on the Si substrate. As for the Ni deposition on Cu, because of their relatively small lattice mismatch (2.6%), LEED images show that the growth is pseudomorphic[15] and no further rotation was observed during *in situ* structural characterization. Finally, Fig. 2(d) shows that the long-range order of the full heterostructure is unaffected by the Cu coating. The LEED patterns of all the deposited layers were also taken at different energies of the primary electron beam. The reflexes were very sharp and did not change their widths with the beam energy. This indicates good crystallographic quality and smoothness of the surface of each layer.

The 30° rotation observed between the Si crystallographic axis and the metallic Cu (and Ni) layers was also confirmed by Kikuchi patterns as reported in Fig. 3. The KED measurements, which allow the investigation of the atomic structure at and below the surface of a solid,[16–18] were taken with the same reverse-view LEED system using an incident electron beam energy of 3 keV. KED is based on the fact that electrons backscattered from surfaces in the keV range show a strong enhancement of intensity along directions defined by atomic rows, because of the forward-scattering effect. The two-dimensional recording of the backscattered electrons reveals the structure near the surface in a way very similar to XPD in real space.[16] KED probes the immediate environment of a particular atomic site (short-range order), and therefore the combination of LEED and KED is ideally suited for the study of epitaxial growth because it provides insight into both long-range order and short-range order of the atomic structure in growing films. On the basis of the reported surface structural results, we are particularly confident of the continuity, well-defined crystal orientation and absence of an interdiffusion process in our heterostructures.

III. EXPERIMENTAL PROCEDURE: BLS AND MOKE

Brillouin scattering experiments were performed at Perugia University, with the specimen in air, at room temperature. Typical acquisition times of 2 h were needed for most measurements, but the sampling time increased to about 5 h for the Ni films with thickness lower than 2.5 nm because of the reduced Brillouin cross section. A beam of monochromatic light from an Ar^+ laser, operating on a single mode of the 514.5-nm line, was focused onto the surface of the specimen and the backscattered light was analyzed using a Sandercock-type,[1,19,20] $3+3$ tandem Fabry-Pérot interferometer, characterized by a finesse of about 100 and a contrast ratio higher than 5×10^{10}. The magnetic field, ranging between 0.8 and 10 kOe, was applied parallel to the sample surface and perpendicular to the plane of incidence of light.

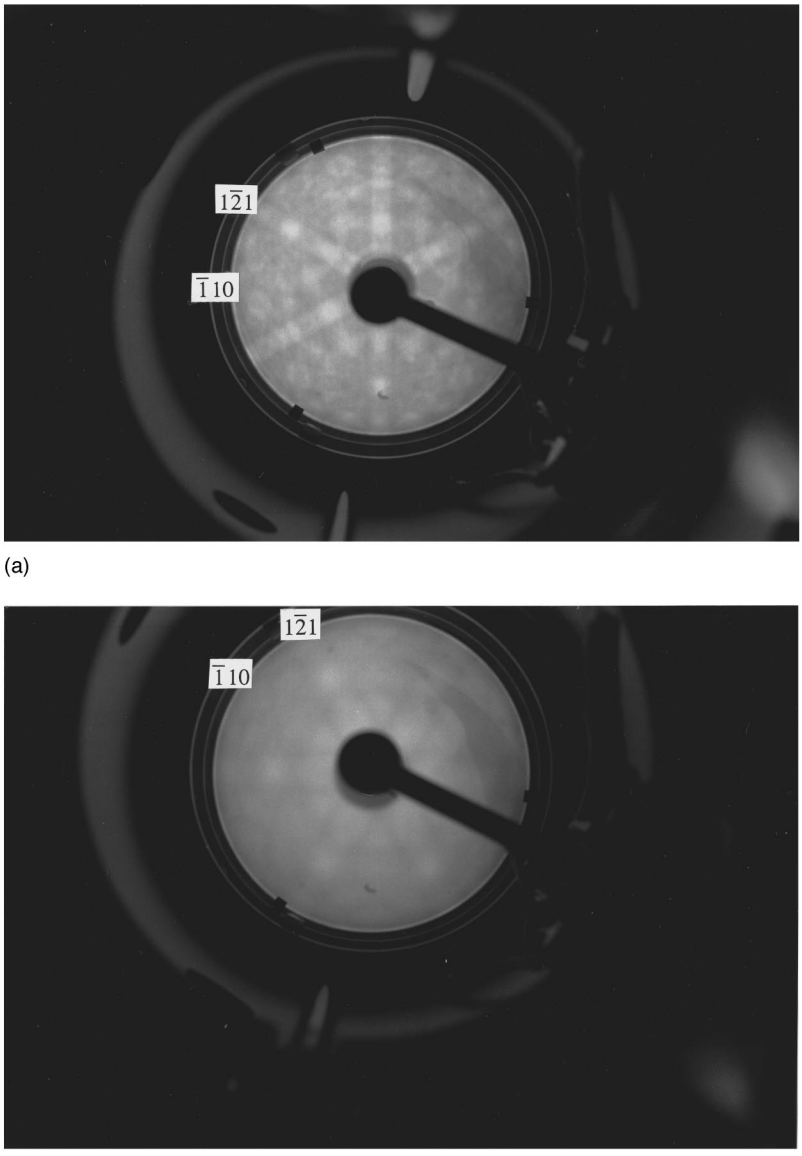

FIG. 3. (a) Kikuchi patterns for the Si(111) 7×7 substrate and (b) for the Cu(111) buffer layer 3.5 nm thick taken for an incident electron beam energy of 3 keV. The 30° relative rotation between the Si and Cu is clearly visible.

The specimen was mounted on a sample holder free to rotate around a vertical axis so that the angle between the spin-wave wave vector and the crystallographic axes of the sample could be varied. Because light scattered by magnons is cross-polarized with respect to the incident light, an analyzer was placed at the entrance of the interferometer in order to stop both the elastically scattered light and the light scattered by phonons. The detector was a SPCM-100-PQ photodiode with a dark count lower than 3 counts/s. To avoid saturation of the photon-counting system, a mechanical shutter at the entrance of the interferometer interrupts the primary beam intensity during the scan across the elastic peak, while a much weaker secondary beam is used to maintain the stabilization of the interferometer.[21] In the backscattering interaction geometry, used in our experiments, the conservation of momentum in the photon-magnon interaction implies that the spin-wave wave vector parallel to the film surface is linked to the optical wave vector K_i and to the angle of incidence β by the equation $q_{\parallel}=2K_i\sin\beta$. In our measurements $\beta=45°$ and therefore $q_{\parallel}=1.73\times10^5$ cm^{-1}.

MOKE measurements were performed at University of L'Aquila, at a light incidence angle of 45°. The magnetic field was directed either normal to the sample surface (polar geometry) or parallel to it (longitudinal geometry). The field intensity was varied in the range $(-200, +200)$ Oe in both the geometrical configurations to obtain polarization rotation loops which are directly related to the magnetization loops. Our equipment allowed us to choose any wavelength of the incident light between 0.5 and 2.6 μm. However, for our purpose, we simply selected the wavelength corresponding to the best signal-to-noise ratio, given the characteristics of our experimental setup and the spectral magneto-optical response of the sample. The polarization was detected using a polarization modulation technique, which relies on a 57-kHz commercial photoelastic modulator (PEM-80, Hinds). This gives a very high sensitivity, allowing us to detect rotations

down to less than 10^{-3} deg. All measurements were performed with the sample kept in air, at a controlled temperature (300.0 ± 0.1 K), in order to prevent displacements of the sample itself or its holder during the measurements and consequent misalignment and deviation of the optical beam.

IV. CALCULATION OF SPIN-WAVE MODE FREQUENCIES

In the following we will present the theoretical approaches for calculating the spin-wave frequency in the case of out-of-plane and in-plane magnetized films. In the first section, we will introduce the general equations for the energy contribution for the (111) plane and then we will restrict to the study of the transition of the magnetization from out of plane to in plane. In the second section, an analytical expression for the spin-wave frequency is obtained in the limit of ultrathin film, separating the volume and the surface anisotropy contributions which enter the Landau-Lifshitz equation of motion and the Rado-Weertman boundary conditions, respectively.

A. Out-of-plane magnetized samples

In order to calculate the frequency of the spin-wave modes in our Ni ultrathin films, we apply the theoretical model previously proposed by Stamps and Hillebrands for a film of hexagonal symmetry[10] to the case of the (111) surface of a cubic crystal. This model takes into account both bulk and surface anisotropy and includes the effects of both dipolar and exchange interactions. The magnetization is assumed to lie at a generic orientation with respect to the film plane, because of the presence of a strong out-of-plane magnetic anisotropy. Since the spin waves probed by BLS have wavelength comparable with that of light, i.e., much larger than the lattice parameters, the medium can be considered as a continuum and the discrete nature of the spins can be neglected. The geometry for the spin-wave dispersion calculation was chosen with the x axis normal to the film surfaces and the z axis along the direction of the external field H_0, as shown in Fig. 4. In order to simplify the expression of the Landau-Lifshitz equation of motion, a second coordinate system is defined with the z' axis parallel to the saturation magnetization, at an angle θ from the z axis. The free energy density of the system consists of the following terms: (i) the potential energy density f_p of the magnetization M_s in the external field H_0,

$$f_p = -H_0 M_s \cos\theta \cos(\phi - \phi_H); \tag{1}$$

(ii) the demagnetizing free energy f_d due to finite sample dimensions,

$$f_d = 2\pi M_s^2 \sin^2 \theta; \tag{2}$$

(iii) the volume energy density f_v due to magnetocrystalline anisotropy,

$$f_v = \frac{K_1}{3}\left[1 - 2\cos^2\theta + \frac{7}{4}\cos^4\theta - \sqrt{2}\cos^3\theta \sin\theta \cos(3\phi)\right], \tag{3}$$

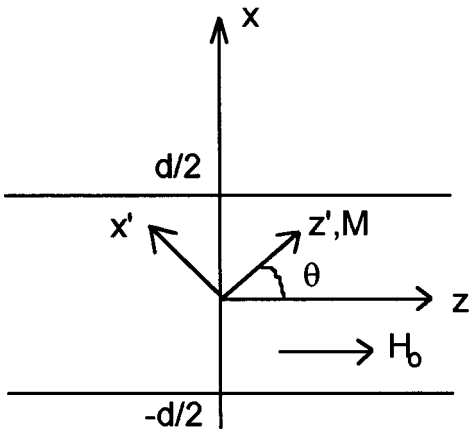

FIG. 4. Coordinate systems used for calculating spin-wave frequencies. The crystal coordinate system (x,y,z) is fixed with respect to the magnetic film, with the x axis normal to the surface and the z axis along the direction of the applied magnetic field H_0. The static magnetization M_s is assumed to be uniform and lies in the xz plane. A primed coordinate system is defined such that M_s lies along the z' axis. The angle between M_s and the z axis is θ.

where ϕ and ϕ_H are the azimuthal angles of M_s and H_0 measured with respect to the crystallographic (110) axis in the film plane and K_1 is the first-order volume-anisotropy constant. [The above expression is directly obtained from the magnetocrystalline energy of a cubic crystal, introducing the direction cosines of the magnetization in a rotated coordinate system with the z' axis along the (111) direction.] Finally, (iv) the free-energy density f_s due to interface anisotropy,[22]

$$f_{\text{inter}} = -K_s \sin^2\theta - \frac{\sqrt{2}}{3} K_p \cos^3\theta \sin\theta \cos(3\phi), \tag{4}$$

has to be considered, where K_s and K_p are the out-of-plane and the in-plane anisotropy constants, respectively. The expression for the in-plane anisotropy energy density reflects the in-plane crystallographic symmetry and is valid even in the case when the magnetization is not in the film plane. Given the sign of the first term in Eq. (4), we follow the convention according to which $K_s > 0$ means an out-of-plane orientation for the magnetization while the negative value of K_s means a preferential in-plane orientation. A simplified expression for the magnetic free energy density of a cubic crystal with (111) orientation can be obtained when the magnetic field is applied along the (121) direction, assuming M_s and H_0 to be collinear. This assumption is reasonable whenever the in-plane anisotropy constant K_p is much lower than the out-of-plane constant K_s, as it will be shown in Sec. V for our Ni films. As a consequence, the dependence on the in-plane azimuthal angle disappears and the magnetic free energy per unit area assumes the following form:

$$F/\sigma = \int dx \left[-H_0 M_s \cos\theta + 2\pi M_s^2 \sin^2\theta + \frac{K_1}{3}\left(1 - 2\cos^2\theta + \frac{7}{4}\cos^4\theta\right)\right] - 2K_s \sin^2\theta, \tag{5}$$

where the factor of 2 in the last term accounts for the two interfaces of the magnetic film. Because we are considering

magnetic films with thickness lower than the exchange correlation length (which in the case of Ni is of about 7 nm), the magnetization can be assumed to be uniform across the film thickness and therefore independent of the x coordinate. This makes it possible the definition of a magnetic free energy per unit volume in the form,

$$F/V=\left[-H_0M_s\cos\theta+2\pi M_s^2\sin^2\theta+\frac{K_1}{3}\times\left(1-2\cos^2\theta+\frac{7}{4}\cos^4\theta\right)\right]-2\frac{K_s}{d}\sin^2\theta. \quad (6)$$

In order to find the equilibrium direction of the magnetization, the minima of the magnetic free energy with respect to the tilt angle θ have to be found. One solution is always $\theta=0$ while the others can be obtained finding the zeros of the third-order equation

$$-\frac{7}{3}K_1\cos^3\theta+\left(4\pi M_s^2+\frac{4}{3}K_1-4\frac{K_s}{d}\right)\cos\theta+H_0M_s=0. \quad (7)$$

This equation gives always a nonphysical solution ($\cos\theta>1$), while one of the other two solutions corresponds to the minimum of the magnetic free energy. For $K_1=0$ the analytical expression of $\cos\theta$ is equal to that obtained in Ref. 10 for a film with hexagonal symmetry, provided that the proper anisotropy constants of an hexagonal medium are used.

In presence of a large out of plane anisotropy, Eq. (7) predicts that the magnetization lies out of plane for zero applied field, while it begins to rotate in the film plane under the action of the field. A critical field $H_{\rm crit}$ can be defined so that for $H>H_{\rm crit}$ the magnetization lies in the film plane. The expression of this critical field, which follows from Eq. (7) with $\cos\theta=1$, is the following:

$$H_{\rm crit}=\frac{\frac{7}{3}K_1-(4\pi M_s^2+\frac{4}{3}K_1-4K_s/d)}{M_s}. \quad (8)$$

Once the direction of the magnetization has been determined, the spin-wave frequency can be calculated by use of a standard procedure which relies upon the resolution of the Landau-Lifshitz equation of motion in the magnetization frame, imposing both the Maxwell and the Rado-Weertman boundary conditions at the film interfaces.[23] The procedure we have followed is discussed in great details by Stamps and Hillebrands,[10] and the spin-wave frequency is obtained finding the zeros of the boundary-condition determinant by means of an appropriate numerical tool. The only difference with respect to the expressions published in Ref. 10, which are valid for a crystal of hexagonal symmetry, is that the anisotropy fields R_x and R_y for a cubic crystal with (111) orientation have the following expressions:

$$R_x=-\frac{K_1}{3M_s}\left[4(2\sin^2\theta-1)+7(1-4\sin^2\theta)\cos^2\theta\right]+\frac{4K_s}{dM_s}(2\sin^2\theta-1), \quad (9)$$

$$R_y=\frac{K_1}{3M_s}\left[4\cos^2\theta-7\cos^4\theta\right]+\frac{4K_s}{dM_s}\sin^2\theta. \quad (10)$$

B. In-plane magnetized samples

We show now that in the ultrathin film approximation, when the magnetization lies along the sample surface, an analytical expression for the long-wavelength spin-wave frequency in the dipolar-exchange regime can be obtained without applying any numerical procedure.[11] The geometry is the same reported in Fig. 4: The magnetic film lies in the y-z plane, and the spin-wave propagation wave vector makes an angle ϕ with the crystallographic (110) axis in the film plane. The theoretical model we are using involves the Landau-Lifshitz equation of motion with an effective field defined as follows:

$$\mathbf{H}_{\rm eff}=\hat{z}H_0+\frac{2A}{M_s}\nabla^2\mathbf{M}-\frac{1}{M_s}\boldsymbol{\nabla}_{\alpha_M}f_v+\mathbf{h}. \quad (11)$$

This expression includes the applied magnetic field H_0, the exchange field where A is the exchange stiffness constant, the magnetocrystalline anisotropy field, and the fluctuating field. We assume that the dynamic components of the fields $\mathbf{m}$ and $\mathbf{h}$ are proportional to $\exp[i(\omega t-q_{\|}x_{\|})]$, where $\mathbf{q}_{\|}$ and $\mathbf{x}_{\|}$ are the component of the spin-wave wave vector and the vector position parallel to the film plane, respectively. A system of two linear equations in the components of $\mathbf{m}$ and $\mathbf{h}$ can be obtained resolving the Landau-Lifshitz equation, that is

$$-i\frac{\omega}{\gamma}m_x=\left[H_0+\frac{2A}{M_s}\left(q_{\|}^2-\frac{\partial^2}{\partial x^2}\right)\right]m_y-M_sh_y+\nabla_{\alpha_y}f_V, \quad (12)$$

$$-i\frac{\omega}{\gamma}m_y=-\left[H_0+\frac{2A}{M_s}\left(q_{\|}^2-\frac{\partial^2}{\partial x^2}\right)\right]m_x+M_sh_x-\nabla_{\alpha_x}f_V, \quad (13)$$

with

$$\nabla_{\alpha_x}f_V=H_\alpha m_x+H_\gamma m_y, \quad (14)$$

$$\nabla_{\alpha_y}f_V=H_\gamma m_x+H_\beta m_y, \quad (15)$$

where H_α, H_β, and H_γ are the volume anisotropy fields and α_i, $i=x,y,z$, are the direction cosines of $\mathbf{M}$. The anisotropy fields can be expressed in terms of the polar coordinates θ and ϕ, which have been already introduced, using the following relations:[24]

$$H_\alpha=\frac{\partial^2}{M_s\partial\theta^2}f_V,\quad H_\beta=\frac{\partial^2}{M_s\partial\phi^2}f_V,\quad H_\gamma=\frac{\partial^2}{M_s\partial\theta\partial\phi}f_V. \quad (16)$$

The analytical expressions for the volume anisotropy fields for the case of (111) cubic film are reported in Table II. Because we are considering long-wavelength spin waves (magnetostatic approximation), the dipolar field $\mathbf{h}$ can be defined by means of a magnetic potential ψ such that $\mathbf{h}=-\boldsymbol{\nabla}\psi$. Introducing plane-wave solutions for the magnetic potential and magnetization inside the film, in the form

TABLE II. Anisotropy volume and interface fields for in-plane magnetized (111)-oriented cubic film.

H_α	H_β	H_γ	$H_{\alpha'}$	$H_{\beta'}$	$H_{\gamma'}$
$-\frac{K_1}{M}$	0	$\frac{\sqrt{2}K_1}{M}\sin(3\phi)$	$-\frac{2K_s}{M}$	0	$\frac{\sqrt{2}K_p}{M}\sin(3\phi)$

$$\psi=(\psi_+e^{\xi x}+\psi_-e^{-\xi x})e^{iq_\parallel x_\parallel}, \tag{17}$$

$$m=[\hat{x}(a_+e^{\xi x}+a_-e^{-\xi x})+\hat{y}(b_+e^{\xi x}+b_-e^{-\xi x})]e^{iq_\parallel x_\parallel}, \tag{18}$$

and substituting the volume anisotropy fields into Eqs. (12) and (13), these can be written as

$$\left(i\frac{\omega}{\gamma}+H_\gamma\right)(a_++a_-)+\left[H_0+H_\beta+\frac{2A}{M_s}(q_\parallel^2-\xi^2)\right](b_+ +b_-)+iq_yM_s(\psi_++\psi_-)=0, \tag{19}$$

$$\left(i\frac{\omega}{\gamma}-H_\gamma\right)(b_++b_-)-\left[H_0+H_\alpha+\frac{2A}{M_s}(q_\parallel^2-\xi^2)\right](a_++a_-)-\xi M_s(\psi_+-\psi_-)=0, \tag{20}$$

where ξ is a decay constant which is yet undetermined. The behavior of the magnetization at the two interfaces of the magnetic film is described by the Rado-Weertman boundary conditions[23,24]

$$\mathbf{M}\times\left[\frac{1}{M_s}\nabla_M f_{\text{inter}}-\frac{2A}{M_s}\frac{\partial\mathbf{M}}{\partial\mathbf{n}}\right]=0\Big|_{x=\pm d/2}, \tag{21}$$

with f_{inter} the interface anisotropy energy density and $\partial/\partial\mathbf{n}$ the partial derivative with respect to the surface normal unit vector. Introducing the anisotropy fields $H_{\alpha'}$, $H_{\beta'}$, and $H_{\gamma'}$, whose expressions are reported in Table II, the above expression generates the following equations:

$$H_{\alpha'}m_x+H_{\gamma'}m_y\pm\frac{2A}{M_s}\frac{\partial m_x}{\partial x}=0, \tag{22}$$

$$H_{\gamma'}m_x+H_{\beta'}m_y\pm\frac{2A}{M_s}\frac{\partial m_y}{\partial x}=0, \tag{23}$$

where the plus sign is for the surface at $x=d/2$ and the minus sign is for the surface at $x=-d/2$. If plane-wave solutions for the magnetization components are introduced and the Rado-Weertman boundary conditions are properly combined, the following expressions can be obtained:

$$\frac{2A}{M_s}\xi(a_++a_-)=-H_{\alpha'}(a_++a_-)\coth(\xi d/2)-H_{\gamma'}(b_++b_-)\coth(\xi d/2), \tag{24}$$

$$\frac{2A}{M_s}\xi(b_++b_-)=-H_{\gamma'}(a_++a_-)\coth(\xi d/2)-H_{\beta'}(b_++b_-)\coth(\xi d/2). \tag{25}$$

These relations can be expanded in powers of $\coth(\xi d/2)$ up to the first order term in $\xi d/2$ and the magnetization components equations assume the form

$$\left(i\frac{\omega}{\gamma}+H_\gamma+\frac{2}{d}H_{\gamma'}\right)(a_++a_-)+\left[H_0+H_\beta+\frac{2A}{M_s}q_\parallel^2+\frac{2}{d}H_{\beta'}\right](b_++b_-)+iq_\gamma M_s(\psi_++\psi_-)=0, \tag{26}$$

$$-\left[H_0+H_\alpha+\frac{2A}{M_s}q_\parallel^2+\frac{2}{d}H_{\alpha'}\right](a_++a_-)+\left(i\frac{\omega}{\gamma}-H_\gamma-\frac{2}{d}H_{\gamma'}\right)(b_++b_-)-\xi M_s(\psi_+-\psi_-)=0. \tag{27}$$

The decay constant ξ can be eliminated considering the electromagnetic boundary conditions for the normal components of $\mathbf{b}=\mathbf{h}_d+4\pi\mathbf{m}$ and the tangential components of $\mathbf{h}$ at the film surfaces ($x=\pm d/2$). If $\nabla\cdot b=0$ is also taken into account, the following expressions to first order in $\xi d/2$ are obtained:

$$\xi(\psi_+-\psi_-)=4\pi\left(\frac{a_++a_-}{1+q_\parallel d/2}\right), \tag{28}$$

$$q_y(\psi_++\psi_-)=4\pi\frac{q_y^2d}{2q_\parallel^2}\left(\frac{b_++b_-}{1+q_\parallel d/2}\right). \tag{29}$$

Substituting these two relations into the equations of motion, one obtains the following equations which are independent of ξ and of the magnetic potential:

$$\left(i\frac{\omega}{\gamma}+H_\gamma+\frac{2}{d}H_{\gamma'}\right)(a_++a_-)+\left[H_0+H_\beta+\frac{2A}{M_s}q_\parallel^2+\frac{2}{d}H_{\beta'}+\frac{4\pi M_sq_y^2d}{2q_\parallel}\frac{1}{1+q_\parallel d/2}\right](b_++b_-)=0, \tag{30}$$

$$\left[H_0+H_\alpha+\frac{2A}{M_s}q_\parallel^2+\frac{2}{d}H_{\alpha'}+4\pi M_s\frac{1}{1+q_\parallel d/2}\right](a_++a_-)-\left(i\frac{\omega}{\gamma}-H_\gamma-\frac{2}{d}H_{\gamma'}\right)(b_++b_-)=0. \tag{31}$$

The spin-wave frequency of the long-wavelength mode, with $q_\parallel d\ll 1$, is then obtained imposing the determinant of the coefficients of the above equations to vanish:

$$\frac{\omega}{\gamma}=\left[\left(H_0+H_\alpha+\frac{2}{d}H_{\alpha'}+\frac{2A}{M_s}q_\parallel^2+4\pi M_s(1-q_\parallel d/2)\right)\times\left(H_0+H_\beta+\frac{2}{d}H_{\beta'}+\frac{2A}{M_s}q_\parallel^2+2\pi M_sq_\parallel d\right)-\left(H_\gamma+\frac{2}{d}H_{\gamma'}\right)^2\right]^{1/2}. \tag{32}$$

This equation shows that using the exchange boundary condition method the interface anisotropy fields are converted into volume anisotropy fields weighed by the ratio $2/d$.[25]

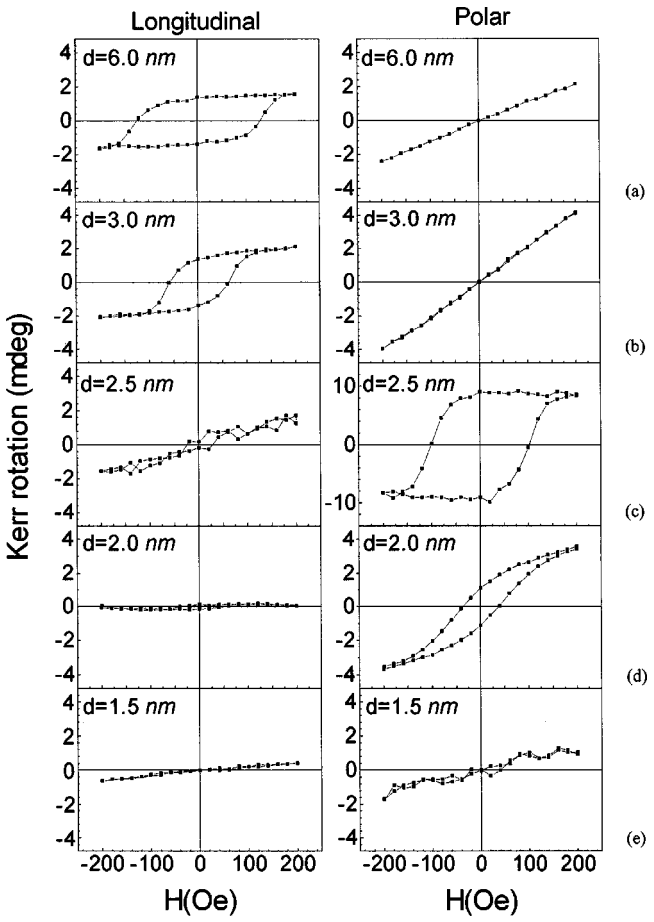

FIG. 5. Longitudinal (left side) and polar (right side) MOKE loops for the Cu/Ni/Cu/Si(111) heterostructures with different thickness d of the Ni film. In the longitudinal configuration the magnetic field is applied along the 121 direction.

V. RESULTS AND DISCUSSIONS

The magnetic characterization of the Cu/Ni/Cu/Si(111) heterostructures has been first performed by *ex situ* MOKE analysis. Measurements in both longitudinal and polar configurations enabled us to gain information about the equilibrium direction of the magnetization in zero applied field. We verified that loops at different wavelength did not have different shapes, but they only implied a different proportionality constant between Kerr rotation and magnetization, as expected from the wavelength dependence of the optical and magneto-optical coefficients. Therefore, wavelength was chosen for each sample in order to optimize the signal-to-noise ratio. Representative MOKE loops obtained in both longitudinal and polar geometry are shown in Figs. 5(a)–5(e). The M-H loops corresponding to the 6.0- and 3.0-nm-thick films, Figs. 5(a) and 5(b), are similar in shape, except for a difference in the coercive field observed in longitudinal geometry which is estimated to be 135 ± 5 and 65 ± 5 Oe, respectively. The remanence of the loops taken with the magnetic field applied in plane is relatively large, which is characteristic of easy axis M-H loops, whereas the loops taken with the field normal to the films exhibit a linear behavior and an insignificant remanence. This indicates that the magnetization easy axis lies in the film plane, in agreement with the expected in-plane alignment of the magnetization at sufficiently large film thickness, due to the magnetostatic energy. The situation changes dramatically when the film thickness is decreased below 3.0 nm, as shown by Figs. 5(c) and 5(d) for the 2.5- and 2.0-nm-thick Ni films. A large hysteresis is now exhibited by the polar M-H loops, indicating that the orientation of the magnetization easy axis is perpendicular to the film plane. However, although the 2.5-nm film is characterized by a polar cycle well saturated and a longitudinal cycle almost linear within the experimental errors, the 2.0-nm film shows a polar cycle not completely saturated at 200 Oe and characterized by a reduced remanence, while the longitudinal loop has a slight hysteresis. The data relative to the 1.5-nm-thick Ni film are affected by a large amount of noise caused by the small M-O signal and need a more accurate interpretation. First of all, we notice that both polar and longitudinal cycles appear to be linear in the range of field shown in Fig. 5(e), i.e., up to 200 Oe. However, polar measurements performed with an applied magnetic field up to 3300 Oe give evidence of a hysteresis, corresponding to a coercive field greater than 100 Oe. This behavior of the 1.5-nm-thick film, together with the above-noted reduction of the remanence in the 2.0-nm-thick film with respect to the 2.5-nm-thick film, can be attributed to the progressive appearance, on reducing the film thickness, of a multidomain structure with the magnetization pointing into and out of the film plane, as already observed in ultrathin Cu/Ni/Cu/Si(001) films by Bochi *et al.*, using magnetic force microscopy.[26] In particular, it was shown that the multidomain structure could be removed approaching a single-domain state, only exposing the sample to magnetic fields as large as several kOe. The vanishing of the remanence in the low-field loop for the 1.5-nm-thick film, Fig. 5(e), indicates that the up and down domains cover comparable surface areas, a situation which is typical of film thicknesses close to the critical value below which the magnetization switches from the perpendicular to the in-plane orientation. Such a transition was actually observed in previous studies of Cu/Ni/Cu(111) sandwiches as the Ni thickness was reduced below the critical value of about 1.3–1.4 nm.[27,28]

Concerning the BLS measurements, we first investigated the dispersion of the spin-wave frequency as a function of the magnetic field applied parallel to the film plane. A representative sequence of spectra from the thicker Ni film (sample No. 5) is shown in Fig. 6. Due to the low ratio between the film thickness and the magnon wavelength, only the peak corresponding to the Damon-Eshbach (DE) surface mode is present in the spectra, since bulk standing modes are at higher frequencies, not accessible in our experiment. The peak exhibits a marked Stokes–anti-Stokes asymmetry, which is typical of magnons in thin ferromagnetic films of absorptive materials.[29] The experimental data relative to the frequency dispersion of the DE peak vs the applied field have been fitted to the curves calculated by the theory described in Sec. IV A, taking the saturation magnetization M_s and the out-of-plane anisotropy constant K_s as fit parameters. The Ni bulk anisotropy constant, the exchange stiffness constant, and the gyromagnetic ratio were kept fixed at the values given in the literature ($K_1=-5.1\times10^4$ erg/cm^3, $A=7.25\times10^{-7}$ erg/cm, $\gamma=1.917\times10^7$ Hz/Oe).[30,20,31] The obtained results are shown in Table I, while the best-fit curves are reported in Fig. 7 together with the experimental

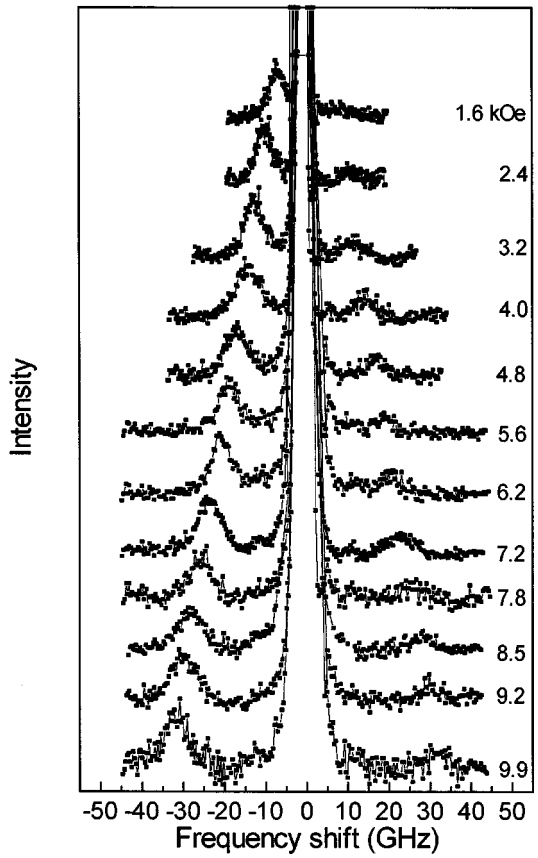

FIG. 6. Brillouin spectra from sample No. 4 as a function of the magnetic field applied along the 121 direction in the range between 1.6 and 9.9 kOe. The angle of incidence of light is 45°.

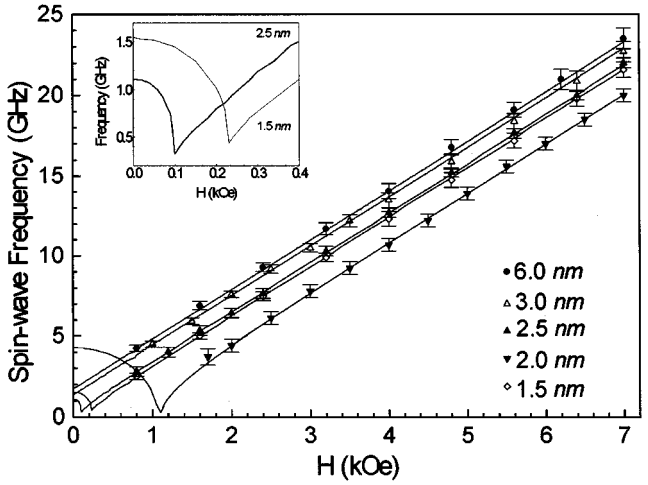

FIG. 7. Magnetic field dependence of the surface mode frequency for Cu/Ni/Cu/Si(111) heterostructures with different thickness of the Ni layer. The spin-wave frequency for the Ni films 6.0 and 3.0 nm thick monotonously increases with the applied magnetic field, while for the thinner Ni films the frequency dispersion has a characteristic minimum at a critical field H_{crit}. The inset shows a magnification of the characteristic dip in the spin-wave frequency for samples Nos. 1 and 3.

points for all the specimens analyzed. The values obtained for the saturation magnetization are in good agreement with those already measured in thick Ni films by other authors.[32] We notice that for the two thicker samples the calculated spin-wave frequency monotonously increases with a quasilinear dependence on the applied field, reflecting an in-plane orientation of the magnetization. For the three thinner samples, the frequency curves present a characteristic minimum at the critical field H_{crit} whose value is about 220, 1100, and 100 Oe, for samples with thicknesses of 1.5, 2.0, and 2.5 nm, respectively. As the applied field H_0 is increased from zero, the magnetization begins to rotate until it is forced in the film plane for $H_0 = H_{crit}$; for higher magnetic fields, the magnetization lies in the film plane and this results in a quasilinear increase of the spin-wave frequency. This behavior is qualitatively similar to that observed in the past in Fe films and indicates that the film is perpendicularly magnetized in zero applied field,[2] consistently with the MOKE results. Unfortunately, we could not reveal the spin wave neither in proximity of H_{crit} where its frequency falls below the range accessible by our apparatus nor in the limit of zero applied field, because of the vanishing Brillouin cross section.[33] In order to clarify the analysis of the magnetization orientation, we used the values of the magnetic parameters obtained from the fitting procedure to calculate the magnetic free energy of the system, as a function of the external applied field. The results of such calculation, for sample Nos. 5 and 1, are shown in Fig. 8. It can be seen that in the case of the thicker sample (No. 5), the magnetic free energy for in-plane magnetization is lower than that corresponding to out-of-plane magnetization, whatever the value of the external applied field. On the other hand, for the thinner sample (No. 1), the out-of-plane magnetization orientation has a lower energy only for applied fields lower than 220 Oe, while at higher fields the in-plane magnetized state is preferred.

As a second step of our BLS investigation, we have studied the frequency dispersion of the spin wave as a function of the direction of the magnon wave vector on the surface plane. The applied field is kept fixed at a value of 4000 Oe, which gives assurance of an in-plane magnetization for all the specimens. In Fig. 9 the frequency of the surface spin wave in samples Nos. 3, 4, and 5 is plotted as a function of the angle ϕ between the applied field direction and the (110) axis (for the thinner samples, Nos. 1 and 2, we did not perform this kind of analysis because of the very low Brillouin cross section). It can be seen that all the sets of data exhibit a clear oscillating behavior with sixfold periodicity, because of the presence of an appreciable anisotropy which reflects the crystallographic symmetry of the Ni (111) plane. In order to reproduce the observed angular dependence of the spin-wave frequency, we used the analytical expression for the spin-wave frequency contained in Eq. (32). In this respect, we notice that the amplitude of the oscillation of the spin-wave frequency with the angle ϕ essentially depends on the term $H_{\gamma'}$, which contains the in-plane surface anisotropy constant K_p, while the influence of the bulk term H_γ, containing the first-order Ni bulk constant K_1, is negligible. The solid line curves of Fig. 9 have been obtained by a best-fit procedure, assuming K_p as a variable parameter, with the other magnetic constants fixed at the values found in the previous analysis of the spin-wave dispersion with the magnetic field. The numerical values we have obtained for the in-plane anisotropy constant are shown in the last column of Table I.

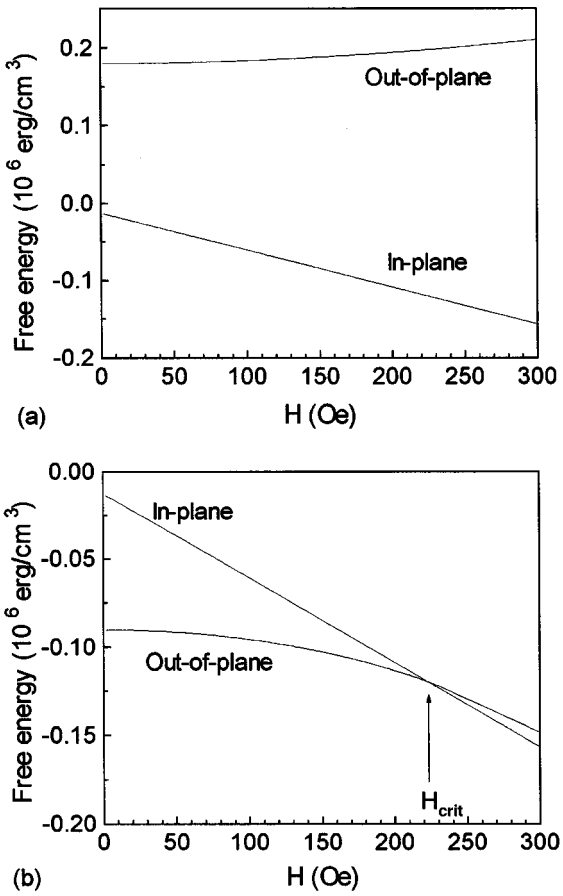

FIG. 8. Magnetic free energy density as a function of the applied field for sample No. 5 (a) and sample No. 1 (b) calculated using the theory described in Sec. IV A. For the thicker sample (No. 5), the equilibrium direction of the magnetization is in the film plane for any values of the applied field. Instead, for sample No. 1, the out-of-plane orientation corresponds to the equilibrium configuration of the system for applied fields below about 220 Oe, while at higher fields the magnetization is forced into the film plane.

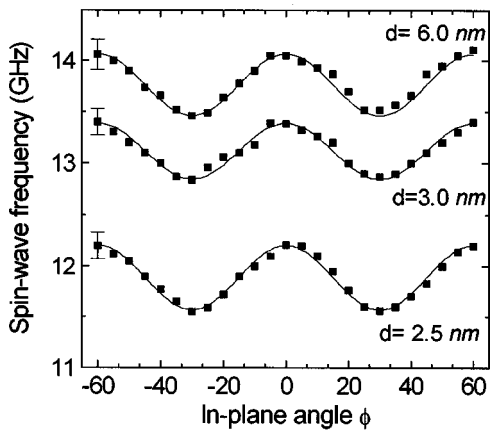

FIG. 9. Spin-wave mode frequencies are plotted for samples Nos. 5, 4, and 3. The magnetic field of 4.0 kOe was applied at different orientations in the plane of the film and the frequencies are plotted against the angle between the applied field and the 110 axis. Typical error bars are shown on the left for each data set.

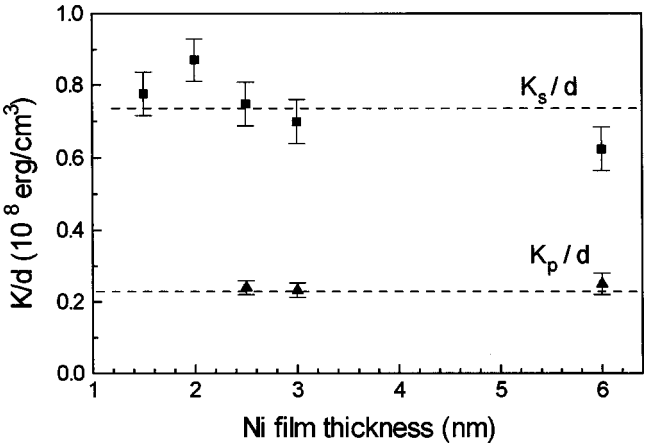

FIG. 10. Thickness dependence of the out-of-plane (K_s) and in-plane (K_p) magnetic anisotropy constants divided by the Ni film thickness (d).

As a general comment on the results obtained, we notice that for all the specimens investigated the values obtained for K_s are positive. This indicates that the interface anisotropy energy always tends to align the magnetization out of the film plane, i.e., along the (111) crystallographic axis, which is an easy axis for bulk Ni. In addition, the values of both K_s and K_p, far from being constant, increase with the film thickness in an almost linear way, as seen in Table I. This can be also seen in Fig. 10 where the ratios K_s/d and K_p/d, which enter the expressions of the spin-wave frequency, are seen to be almost independent of the film thickness d. This suggests that the physical origin of magnetic anisotropy in our system is mainly magnetoelastic, i.e., induced by the strain arising from the pseudomorphic growth of Ni on Cu. As a fact, in the pseudomorphic growth regime the strain can be considered as independent of thickness and hence magnetoelastic anisotropy contributions appear as volume, i.e., thickness-independent, contributions. However, the values of K_s/d for the three thinner specimens are slightly larger than those relative to the two thicker films and this is sufficient to change the magnetization orientation from in plane to out of plane, as observed directly by MOKE measurements. In particular sample No. 2 has the highest value of K_s/d and this reflects in the highest value of H_{crit}.

VI. CONCLUSIONS

We have successfully grown epitaxial Ni(111) ultrathin films of different thickness on Si(111) substrates with Cu buffer and capping layers. The static magnetic properties of these films have been investigated by use of MOKE. This analysis has shown that the magnetization lies in the film plane for films 3 and 6 nm thick, while it switches along the normal to the film for lower thickness. The dynamic magnetic properties were then studied by a detailed BLS investigation of the frequency dispersion of the surface spin wave as a function of the applied magnetic field, which enabled us to determine the out-of-plane magnetic anisotropy constant. The interpretation of BLS data was accomplished using a macroscopic model which takes into account both dipolar and exchange interactions, as well as bulk and interface anisotropy for the (111) plane of a cubic crystal. In a second

step of our BLS investigation, we measured the spin-wave frequency as a function of the wave vector direction on the surface plane. This analysis gave evidence of a rather marked dependence of the frequency on the wave vector direction, with a sixfold periodicity, and enabled us to determine the in-plane anisotropy constant. To this respect, we stress that the (111) plane is unique among the principal planes of cubic crystals because the variation of the magnetocrystalline bulk anisotropy is greatly reduced if compared to other planes. As a consequence, a precise evaluation of the in-plane interface anisotropy constant is directly attained from the analysis of the spin-wave frequency. The observed dependence of both the in-plane and the out-of-plane anisotropy constants on the film thickness indicates that the magnetic anisotropy is mainly of magnetoelastic origin, due to the pseudomorphic growth of Ni on the Cu buffer layer.

ACKNOWLEDGMENTS

The authors would like to thank Professor B. Hillebrands and Professor R. L. Stamps for helpful discussions and continuing support. We also thank Dr. D. Fioretto for the help given in developing the computer program used for the spin-wave frequency calculation and S. Fusari for samples preparation.

[1] J. R. Dutcher, in *Linear and Nonlinear Spin Waves in Magnetic Films and Superlattices*, edited by M. G. Cottam (World Scientific, Singapore, 1994), p. 287.
[2] J. R. Dutcher, B. Heinrich, J. F. Cochran, D. A. Steigerwald, and W. F. Egelhoff, Jr., J. Appl. Phys. **63**, 3464 (1988).
[3] J. F. Cochran, in *Ultrathin Magnetic Structures II*, edited by B. Heinrich and J. A. C. Bland (Springer-Verlag, Berlin, 1994), p. 222.
[4] D. Kerkmann, J. A. Wolf, D. Pescia, Th. Woike, and P. Grunberg, Solid State Commun. **72**, 963 (1989).
[5] J. R. Sandercock and W. Wettling, IEEE Trans. Magn. **14**, 442 (1978).
[6] G. Rossi, Surf. Sci. Rep. **7**, 1 (1987), and references therein.
[7] B. P. Tonner, J. Zhang, X. Chen, Z.-L. Han, G. R. Harp, and D. K. Saldin, J. Vac. Sci. Technol. B **10**, 2082 (1992).
[8] C. A. Chang, Phys. Rev. B **42**, 11 946 (1990).
[9] B. Hillebrands, P. Krams, J. Fassbender, C. Mathieu, G. Guntherodt, R. Jungblut, and M. T. Johnson, Acta Phys. Pol. A **85**, 179 (1994).
[10] R. L. Stamps and B. Hillebrands, Phys. Rev. B **43**, 3532 (1991).
[11] R. L. Stamps and B. Hillebrands, Phys. Rev. B **44**, 12 417 (1991).
[12] B. Hillebrands, Phys. Rev. B **41**, 530 (1990).
[13] M. De Crescenzi, R. Gunnella, R. Bernardini, M. De Marco, and I. Davoli, Phys. Rev. B **52**, 1806 (1995).
[14] S. A. Chambers, S. B. Anderson, and J. H. Weaver, Phys. Rev. B **32**, 581 (1985).
[15] S. A. Chambers, H. W. Chen, I. H. Vitomirov, S. B. Anderson, and J. H. Weaver Phys. Rev. B **33**, 8810 (1986); S. A. Chambers, Surf. Sci. Rep. **16**, 261 (1992).
[16] Z.-L. Han, S. Hardcastle, G. R. Harp, H. Li, X.-D. Wang, J. Zhan, and B. P. Tonner, Surf. Sci. **258**, 313 (1991).
[17] M. Erbudak, M. Hochstrasser, and E. Wetli, Mod. Phys. Lett. B **8**, 1759 (1994).
[18] H. Zhao, S. P. Tear, and H. Jones, Phys. Rev. B **52**, 8439 (1995).
[19] J. R. Sandercock, in *Light Scattering in Solids III*, edited by M. Cardona and G. Guntherodt, Springer Series in Topics in Applied Physics Vol. 51 (Springer-Verlag, Berlin, 1982), p. 173.
[20] P. Grunberg, in *Light Scattering in Solids V*, edited by M. Cardona and G. Guntherodt, Springer Series in Topics in Applied Physics Vol. 66 (Springer-Verlag, Berlin, 1989), p. 303.
[21] G. Gubbiotti, G. Carlotti, and G. Socino, in *Nanophase Materials*, edited by E. Bonetti and D. Fiorani (Trans Tech, Zurich, 1997), p. 215.
[22] This expression of the interface energy density is obtained from the magnetocrystalline energy density, retaining only the part which depends on the in-plane angle ϕ.
[23] G. T. Rado and J. R. Weertman, J. Phys. Chem. Solids **11**, 315 (1959).
[24] B. Hillebrands, in *Light Scattering in Solids VII*, edited by M. Cardona and G. Guntherodt, Springer Series in Topics in Applied Physics (Springer-Verlag, Berlin, in press).
[25] G. T. Rado, J. Magn. Magn. Mater. **104**, 1679 (1992).
[26] G. Bochi, C. A. Ballentine, H. E. Inglefield, C. V. Thompson, and R. C. O'Handley, Phys. Rev. B **52**, 7311 (1995).
[27] U. Gradmann, R. Bergoltz, and E. Bergter, IEEE Trans. Magn. **20**, 1840 (1984).
[28] R. Jungblut, M. T. Johnson, J. aan de Stegge, A. Reinders, and F. J. A. den Broeder, J. Appl. Phys. **75**, 6424 (1994).
[29] R. E. Camley, P. Grunberg, and C. M. Mayr, Phys. Rev. B **26**, 2609 (1982).
[30] J. Crangle, *The Magnetic Properties of Matter* (Arnold, London, 1977), p. 112.
[31] E. P. Wohlfarth, in *Ferromagnetic Materials*, edited by E. P. Wohlfarth (North-Holland, Amsterdam, 1980), Vol. 1, p. 35.
[32] P. Grunberg, C. M. Mayr, W. Vach, and M. Grimsditch, J. Magn. Magn. Mater. **28**, 319 (1982).
[33] J. R. Dutcher, J. F. Cochran, I. Jacob, and W. F. Egelhoff, Jr., Phys. Rev. B **39**, 10 430 (1989).